Zoological Journal of the Linnean Society, 2021, **191**, 941–960. With 10 figures.

Two parasitic ciliates (Protozoa: Ciliophora: Phyllopharyngea) isolated from respiratory-mucus of an unhealthy beluga whale: characterization, phylogeny and an assessment of morphological adaptations

DIDI JIN[1†], ZHISHUAI QU[2†], BOJUE WEI[1], DAVID J. S. MONTAGNES[3], XINPENG FAN[4*] and XIANGRUI CHEN[1*]

[1]*School of Marine Sciences, Ningbo University, Ningbo 315211, China*
[2]*Department of Ecology, University of Kaiserslautern, Kaiserslautern 67663, Germany*
[3]*Institue of Integrative Biology, University of Liverpool, Liverpool L69 7ZB, UK*
[4]*School of Life Sciences, East China Normal University, Shanghai 200241, China*

Received 6 March 2020; revised 18 May 2020; accepted for publication 2 July 2020

Ciliates occur in the blowholes of marine mammals, but our understanding of their biology is poor. Consequently, we investigated an infestation of ciliates in an unhealthy, captive beluga whale that was exhibiting accelerated breathing, leukocytosis and expulsion of unusually large amounts of viscous sputum. This sputum contained ~10^4 ciliates mL^{-1} (when healthy, numbers were ten- to 100-fold lower). One known ciliate species, *Planilamina ovata*, is fully characterized, and a new species, ***Kyaroikeus paracetarius* sp. nov.**, is here described. The new species is established based on its larger number of left kineties over its only congener. Sequences of small-subunit rDNA, large-subunit rDNA and ITS1-5.8S-ITS2 regions of these two taxa were used in phylogenetic analyses, inferring that *Kyaroikeus* and *Planilamina* have close affinity with the free-living family Dysteriidae, contradicting their morphology-based assignment to the family Kyaroikeidae. We suggest that Kyaroikeidae be relegated to subfamily status. Finally, by comparing parasitic species with free-living taxa, we suggest how these ciliates have adapted to their unique environment and how they may have initially invaded the host. We provide essential data and concepts for the continued evaluation of ciliate-parasites in whale blowholes.

ADDITIONAL KEYWORDS: disease – *Kyaroikeus paracetarius* – morphology – multigene sequences – new species – parasitism – ultrastructure.

INTRODUCTION

The phylum Ciliophora is ubiquitous and diverse, with in the order of 10 000 species comprising free-living, commensal and parasitic forms (Lynn, 2008; Song *et al.*, 2009; Hu *et al.*, 2019). Although a large number of ciliates are parasites of aquatic invertebrates and fishes, few seem to parasitize aquatic mammals. Of note in this regard are the blood-feeding prostomatean ciliate *Haematophagus megapterae* Woodcock & Lodge, 1921 that infects the baleen plates of humpback, fin and blue whales, and the litostomatean ciliates *Balantidium* Claparède & Lachmann, 1858, found in the large intestine and faeces of sea lions and fin whales (Hermosilla *et al.*, 2015, 2016). Some uncharacterized ciliates are also associated with the skin, blowholes, air sacs, bronchiole, lungs, lymph node and faeces of dolphins and whales (Poynton *et al.*, 2001; McFee & Lipscomb, 2009; Lair *et al.*, 2016).

All of the ciliates associated with marine mammals are thought to elicit low pathogenicity or at least act as opportunists, invading ulcerated areas, especially in cetaceans that are unhealthy (Choi *et al.*, 2003; Gulland *et al.*, 2018). Therefore, to appreciate the

*Corresponding authors. E-mail: xiangruichen@126.com; xpfan@bio.ecnu.edu.cn
†Contributed equally to this work.
[Version of record, published online 3 September 2020; http://zoobank.org/ urn:lsid:zoobank.org:pub:C1B0E492-7846-4103-87E0-A137D16A590D]

impact of ciliates on the health of cetaceans, there is a need to both report cases of such instances and, critically, identify the invasive taxa. To this end we report on the abundance, morphology, phylogenetic position and adaptive traits of one known and one new ciliate species, found at unprecedented abundances in the respiratory tract of a captive beluga whale that was suffering from respiratory problems.

MATERIAL AND METHODS

Sample collection

Samples were collected from a solitary ~10-year-old beluga whale [*Delphinapterus leucas* (Pallas, 1776)], kept in captivity for ~6 years in Ningbo Aquarium, China (Supporting Information, Fig. S1, picture of the white beluga). This intensely managed aquarium is a closed system, with all water recirculated (~18.0 °C, ~28 PSU (practical salinity units), pH 7.8, total nitrogen 0.05 mg L^{-1}, nitrite 0.05 mg L^{-1}) and periodically sterilized. The beluga whale was contained in a 2500 m^3 (about 400 m^2, average water depth 5 m) enclosure. It was fed four times a day, mostly with wild-caught herring and capelin, with a total amount of about 18 kg per day.

In May 2017, the beluga whale exhibited abnormal behaviour, frequently floating on the water or lying sideways, sometimes standing upright by the side of the pool and rubbing the wall with the outer margin of its blowhole. Its breathing frequency increased to four per minute (normally one to three per minute), and it often exhaled aggressively to expel mucus, which contained exfoliated epithelial tissue. Moreover, a blood test indicated leukocytosis (conducted by the veterinarian of the aquarium; Supporting Information, Data S1, blood test index of beluga whale), a clear sign of poor health (Norman *et al.*, 2012). Expelled mucus (including epithelial tissue) was obtained using two methods: (1) when the amount of released mucus with epithelial tissue was large, the floating mucus was collected directly into a container; (2) when floating mucus was not available, nasal mucus was collected from the host directly; the beluga whale was encouraged to rest its head on the pool bank, and after ~five exhalations, the veterinarian collected the mucus (Supporting Information, Fig. S1C; Ma *et al.*, 2006).

The mucus with epithelial tissue was directly examined using a stereomicroscope; ciliates were collected using a micropipette and observed by compound microscopy. Abundance was determined by placing 50 μL of mucus, containing flocs of epithelial tissue, on a microscope slide and counting cells. About 200 individuals were isolated and examined following the recommendations of Warren *et al.* (2017), as outlined below. The movement and feeding of the new species were recorded (Supporting Information, Video S1, filming of movement and feeding).

In December 2019, the beluga whale had fully recovered and was in a healthy state (i.e. no abnormal behaviour, blood tests indicated good health, no mucus was expelled in the water and there was little exfoliated epithelial tissue in the mucus; Supporting Information, Fig. S2). At this time, to assess for abundance of ciliates, the mucus was collected directly from the blowhole four times, one week apart.

Optical microscopy and identification

Immediately after collecting mucus, the live morphology of the ciliates was studied using a compound microscope equipped with differential interference contrast. The ciliary pattern and nuclear apparatus were revealed by protargol staining (Wilbert, 1975), using protargol synthesized following the protocol of Pan *et al.* (2013). Morphometric measurements were conducted at a magnification of 1000×. Illustrations of the stained specimens were made with the aid of a camera lucida. Terminology followed Ma *et al.* (2006), Lynn (2008) and Chen *et al.* (2016).

Scanning and transmission electron microscopy (SEM and TEM)

SEM and TEM studies were only conducted on the new species of *Kyaroikeus* Sniezek, 1995, because preparations for *Planilamina ovata* Ma *et al.*, 2006 failed. The procedures of SEM mainly follow Ma *et al.* (2016). Cells were fixed in 2.5% glutaraldehyde and stored at 4 °C. Subsequently, cells were washed three times in 0.1 mol/L phosphate buffer (pH 7.0) to remove fixative. After alcohol dehydrations and critical point drying by CO_2 (Leica EM CPD300), cells were coated with platinum in Leica EMACE600. Observations were made using a Hitachi S-4800 scanning electron microscope with accelerating voltage of 3.0–5.0 kV.

TEM preparation also follows Ma *et al.* (2016): 2.5% glutaraldehyde fixed cells were washed and post-fixed in 1% phosphate buffered OsO_4 for 1 h at 4 °C. After three washes in the cacodylate buffer, specimens were processed through alcohol dehydrations and acetone dehydrations. Then cells were embedded in Epon 12 and polymerized at 37 °C for 16 h, 45 °C for 24 h and 60 °C for 48 h. Thin sections were placed on copper grids using uranyl acetate and lead citrate for staining. These were observed under a Hitachi HT7700 transmission electron microscope with accelerating voltage of 100 kV.

DNA EXTRACTION, PCR AND MULTI-GENE SEQUENCING

Clonal cultures could not be established. Instead, for each species, cells were collected, optically identified and single cells were isolated. These cells were washed four times in filtered habitat water (0.22 µm-pore size membrane, Millipore, USA), washed two times in ultra-pure water and then placed in 1.5-mL microfuge tubes with ~45 µL of buffer. For both species, this process was repeated on three dates (2 May, 2017; 4 June, 2017; 1 January, 2018), providing sequence data for the equivalent of three clonal isolates per species. Genomic deoxyribo necleic acid (DNA) was extracted following the manufacturer's instructions (Dneasy Blood and Tissue Kit, Qiagen, Hilden, Germany). The small-subunit (SSU) rDNA was amplified with the universal eukaryotic primers 18SF (5′-AAC CTG GTT GAT CCT GCC AGT-3′) and 18SR (5′-TGA TCC TTC TGC AGG TTC ACC TAC-3′) (Medlin *et al.*, 1988). A fragment of ~500 bp, containing the internal transcribed spacer regions 1 and 2 (ITS1 and ITS2) and 5.8S ribosomal gene, was amplified using primers 5.8SF (5′-GTA GGT GAA CCT GCG GAA GGA TC-3′) and 5.8SR (5′-CTG ATA TGC TTA AGT TCA GCG G-3′) (Yi *et al.*, 2009). The large-subunit (LSU) rDNA was amplified using the primers 28S-F3 (5′-TAC TGA TAT GCT TAA GTT CAG CGG-3′) and 28S-R2 (5′-AAC CTT GGA GAC CTG AT-3′) (Moreira *et al.*, 2007).

Polymerase chain reaction (PCR) conditions were the same for the three DNA segments and were as follows: (1) initial denaturation for 30 s at 98 °C; (2) 35 cycles of 10 s denaturation at 98 °C, 20 s primer annealing at 56 °C and 100 s primer elongation at 72 °C; and (3) final primer elongation for 120 s at 72 °C. Q5 Hot Start High-Fidelity DNA Polymerase (NEB Co, Ltd, M0493, Beijing) was used to minimize the possibility of PCR amplification errors. Purifying of PCR products, cloning and sequencing were performed (Wang *et al.*, 2017).

PHYLOGENETIC ANALYSES

Six new sequences (SSU rDNA, ITS1-5.8S-ITS2 region and LSU rDNA) of the new *Kyaroikeus* species and *Planilamina ovata* were sequenced and are provided here. Other sequences used in our phylogenetic analyses were obtained from NCBI GenBank database, including: (1) SSU rDNA sequences of 35 dysteriids, 41 chlamydodontids and six suctorians; (2) ITS1-5.8S-ITS2 region sequences of one dysteriid, five chlamydodontids and two suctorians; (3) LSU rDNA sequences of one dysteriid, three chlamydodontids and two suctorians. The suctorians mentioned above were used as outgroup taxa, because the subclass Suctoria is phylogenetically close to the subclass Cyrtophoria.

Sequences were aligned using Clustal W implemented in BIOEDIT v.7.1.3.0 using the default parameters (Hall, 1999). The resulting alignments were manually refined by trimming both ends. Maximum likelihood (ML) analyses were conducted on CIPRES Science Gateway with RAxML-HPC2 on XSEDE v.8.2.4 (Stamatakis *et al.*, 2008) using the GTR+I+G model as optical according to the AIC criterion by ModelTest v.3.4 (Posada & Crandall, 1998). Support for the best ML tree was from 1000 bootstrap replicates. A Bayesian inference (BI) analysis was performed on CIPRES Science Gateway with MrBayes on XSEDE v.3.2.6 (Ronquist & Huelsenbeck, 2003) using the GTR+I+G model (selected by MrModelTest v.2.2) (Nylander, 2004). The chain length of Markov chain Monte Carlo simulations was 10^6 generations with a sampling frequency of every 100^{th} generation. The first 25% of the sampled trees was discarded as burn-in. Phylogenetic trees were visualized via MEGA v.5.0 (Tamura *et al.*, 2011) and TreeView v.1.6.6 (Page, 1996). Systematic classification mainly followed Lynn (2008), Gao *et al.* (2016), and Chen *et al.* (2016).

RESULTS

Two ciliate species were abundant in the mucus of the unhealthy beluga whale: a new species of *Kyaroikeus*, described below (~ 2.5×10^4 mL^{-1}) and *Planilamina ovata* (~ 5.0×10^3 mL^{-1}). These ciliates were also found in the mucus when the beluga whale was healthy, but at much lower numbers: *Kyaroikeus* sp. (~ 2×10^3 mL^{-1}) with *P. ovata* being very rare (< 1×10^2 mL^{-1}) or absent. The ciliates always attached to the surface of the flocs of exfoliated epithelial tissue and fed on the epithelial cells.

All isolated ciliates died within 24 h of leaving the host, regardless of being maintained at 18 °C (water temperature), 25 °C (air temperature) or 35 °C (host body temperature) in mucus samples or mucus diluted to different salinities (0, 5, 10, 15, 20, 28 PSU) (Supporting Information, Data S2, cultivation data of the new species). Therefore, we were not able to culture either taxa. However, it was possible to isolate individuals of both taxa, identify *P. ovata* and provide a re-description of it, and provide a formal, detailed description of the new species. To this end, three isolates of *Kyaroikeus* and three isolates of *Planilamina* were made on different dates (see Methods). DNA sequences isolated from replicate clones were identical, and the two species were distinct.

SYSTEMATICS

ORDER DYSTERIIDA DEROUX, 1976

FAMILY KYAROIKEIDAE SNIEZEK & COATS, 1996

KYAROIKEUS SNIEZEK *ET AL.*, 1995

***KYAROIKEUS PARACETARIUS*, SP. NOV.**

(FIGS 1–5; TABLE 1)

Zoobank: urn:lsid:zoobank.org:act:199C1DAD-F159-4EA7-ACB2-C03492F12B00.

Diagnosis: Size 150–400 × 20–40 μm *in vivo*; spindle-shaped; deep oral cavity composed of a pre-oral kinety and two circumoral kineties; no nematodesmal rods; 37–69 right kineties, seven to 13 left kineties; four kinetofragments located near equatorial position; equatorial fragment positioned next to the middle part of the rightmost right kinety; non-ciliated stripe underlain by 11–16 fibrous tracks; a bifurcated secretory organelle opened at the tip of podite; one ovoid macronucleus.

Host: Delphinapterus leucas (beluga whale).

Etymology: The species name *paracetarius* is a composite of the Greek prefix παρα-, beside, and κήτος, a whale or sea monster, referring to the species-group name *cetarius*, indicating that this new species is morphologically similar to *Kyaroikeus cetarius* Sniezek, 1995.

Type material: One slide with a protargol-stained holotype specimen (indicated with a black circle of ink on the coverslip) and several paratype specimens has been deposited in the Laboratory of Protistology, Ocean University of China (OUC) with registration number LJ-I-20170502-01. Two slides with protargol-stained paratype specimens were deposited in the collection of Ningbo University (registration numbers: LJ-I-20170502-02, LJ-I-20170502-03).

General morphology and ciliary pattern: The body size is 150–400 × 20–40 μm *in vivo* and 150–365 × 35–80 μm after protargol staining. It has a long, spindle-shaped body with a length–width ratio of ~10:1, neither bilaterally nor dorsoventrally compressed (Figs 1A, B, 2A, 3A). Pellicular ridges are distributed on the surface of the cell, between adjacent somatic kineties; densely packed kinetosomes are located at the base of these ridges (Fig. 3H, I). A conspicuous bipolar, non-ciliated stripe is located on the left ventral surface, 10–30 μm wide (Figs 1C, D, H, 2F, R, 3B–F). Eleven to 16 pellicular folds are situated on the 'naked' stripe and are associated with same number of fibrous tracts that extended along the cell almost from end to end; the leftmost four or five folds and their associated fibres are bent to the right anteriorly; these form a hook-like cap and a subapical depression below (Figs 1J, 3B, C). Remaining folds extended from this depression to the posterior end of the body. The oral cavity is located in the anterior quarter of the cell (Figs 1J, 2O, P). A lip-like structure on the right side of the oral cavity and 13–29 right kineties end here. Consequently, the lip-like region is covered with dense cilia (Figs 1A–F, H, 2A, B, O, R, green region). The cytostome is elliptical in outline and positioned at about the anterior one-third of the cell, beneath the depression of the oral cavity (Figs 1J, 2B, O). Cytoplasm is colourless, filled with a few lipid droplets and numerous food vacuoles containing unidentified amorphous inclusions in the posterior end of the cell. A contractile vacuole is not detected.

The single macronucleus is heteromerous and ovoid, about 35 × 20 μm after protargol impregnation, located mid-body (Figs 1I, 2M). A micronucleus is not detected. A prominent podite is broadly cone-shaped, located at the posterior end of the cell (Figs 1A, H, I, 3A, J), about 10 μm in length *in vivo* (Fig. 2A, F). Podite contains a bifurcated secretory organelle, which has an opening (0.5–1.0 μm across) at its tip; an obvious attachment thread (> 100 μm long) is secreted from the podite opening, forming a strong connection with the substrate (Figs 1A, 2E). Ciliates are usually attached to the surface of flocs of exfoliated epithelial tissue by the podite and attachment thread. Cells tend to rotate through flocs of epithelial tissue. The ciliary pattern (Figs 1H–J, 2F–R) comprises of 49–79 somatic kineties, including 37–69 right and seven to 13 left kineties. According to their starting position, right kineties include three parts: (1) the right part of right kineties originates from the right of circumoral kineties and these kineties on the ventral side, with posterior ends gradually shortened from right to left (Fig. 1J); (2) the middle part of right kineties originates from the right of the cell apex on the ventral side and extends on to the dorsal surface, and then posteriorly terminates at a level near the podite (Fig. 1I, J); and (3) the left part of right kineties is located at the cell apex on the dorsal side, and posteriorly extends to the podite, with some extending on to the left field on the ventral side (Fig. 1H, I). Left kineties are densely arranged, located on the left margin of the oral cavity. These kineties are similar in length, and posteriorly ended in the anterior quarter of the cell (Figs 1J, 2O, Q, R). Four kinetofragments are located slightly below the mid-body on the left margin of right kineties (Figs 1H, 2F). The equatorial fragment is composed of five to 28 kinetosomes, positioned next to the middle part of the rightmost right kinety (Fig. 2K, L).

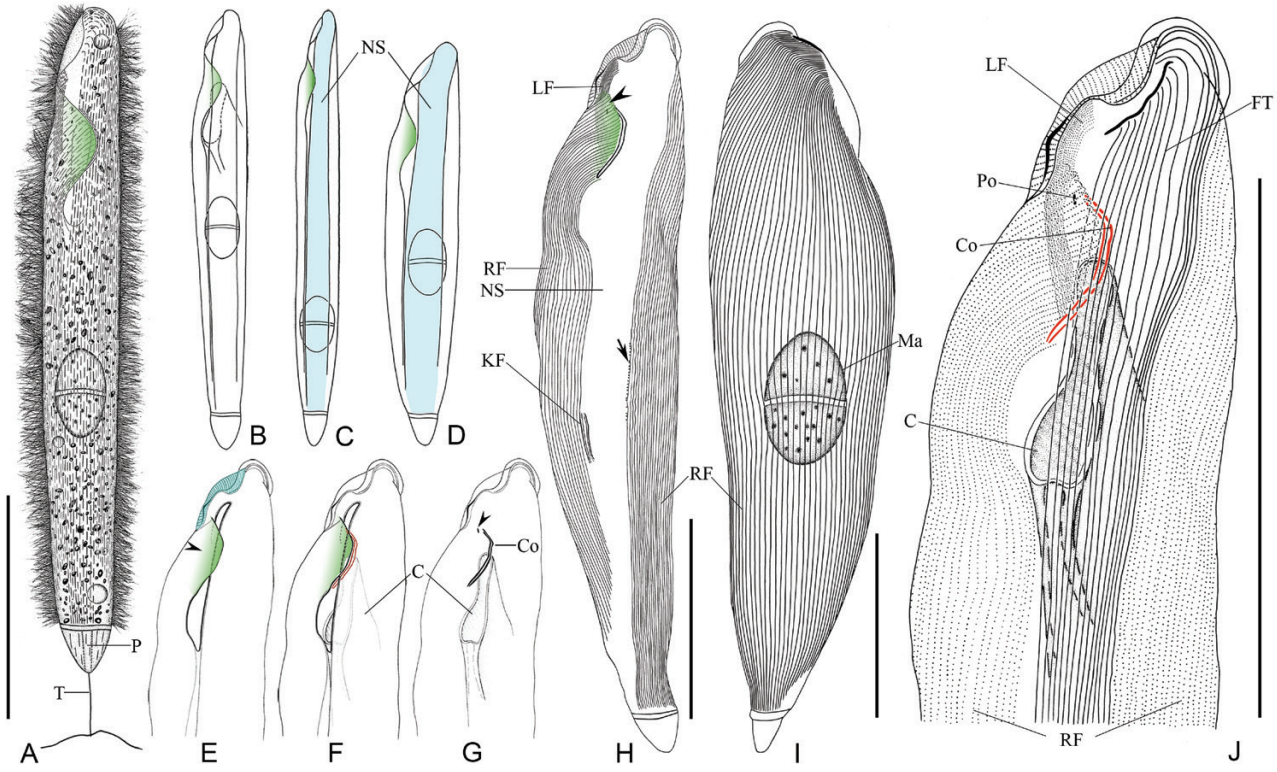

Figure 1. *Kyaroikeus paracetarius* from life (A–D) and after protargol impregnation (E–J). A, ventral view to show the body shape, densely arranged cilia, lip-like structure on the right side of oral cavity (green region), the podite and the attachment thread. B–D, variants of cell shape. E, the oral region: the blue area indicates the kineties of right field on cell apex and the arrowhead indicates the lip-like structure. F, the cytostome and the circumoral kineties (brown lines). G, the oral region, to show the pre-oral kinety (arrowhead) and circumoral kineties. H, I, ventral (H) and dorsal (I) views of infraciliature: the arrowhead indicates the lip-like structure and the arrow indicates the equatorial fragment. J, enlargement of the anterior ventral part of infraciliature to show details of the oral structure, right and left somatic kineties and non-ciliated stripes. Abbreviations: C, cytostome; Co, circumoral kineties; FT, fibrous tracts; KF, kinetofragments; LF, left field; Ma, macronucleus; NS, non-ciliated stripe; P, podite; Po, pre-oral kinety; RF, right field; T, attachment thread. Scale bars = 60 μm (A, H–J).

The oral ciliature is composed of a tiny pre-oral kinety (~2 μm long) and two parallel circumoral kineties (~20 μm long) (Figs 1G, J, 2O, P, R, 3D, G); the former is located on the anterior-right of the cavity and the latter at mid-cavity. Anterior ends of circumoral kineties are close to the pre-oral kinety (Figs 1G, J, 2R). The cytopharynx is reinforced by argentophilic fibres and is extended to mid-body with the posterior end obviously curved (Fig. 2P); no nematodesmal rods are found.

Fine structures: Each of the circumoral kineties is composed of monokinetids (Fig. 4E). The cytopharyngeal tube consists of ~180 cytostomal lamellae (Fig. 4A, B, D), which are bar-like and oriented obliquely to the centre of the tube, forming an enclosed circle when viewed in cross-section. These lamellae are possibly heterogenous, as speculated from the morphology shown in cross-section: about two thirds of them are thinner in their distal ends, while the others are of uniform thickness (Fig. 4B, D).

The pellicle can be recognized as a ciliated area and a non-ciliated stripe in both SEM-prepared specimens and TEM sections. In the ciliated area, the pellicular ridges are arranged intrakinetally (Fig. 3H, I). Each ridge contains a row of postciliary microtubules (Fig. 4C). Parasomal sacs occur right of kinetosomes at the base of the pellicular ridge (Fig. 4C). In the non-ciliated area, the pellicular folds are ~2 μm high, containing four or five (mostly five) strata of microtubules beneath the pellicle (Figs 4H, I, 5), which correspond with the fibrous tracts revealed after protargol staining (Figs 1J, 2R). The microtubules are highly organized: each stratum is arranged in an arch

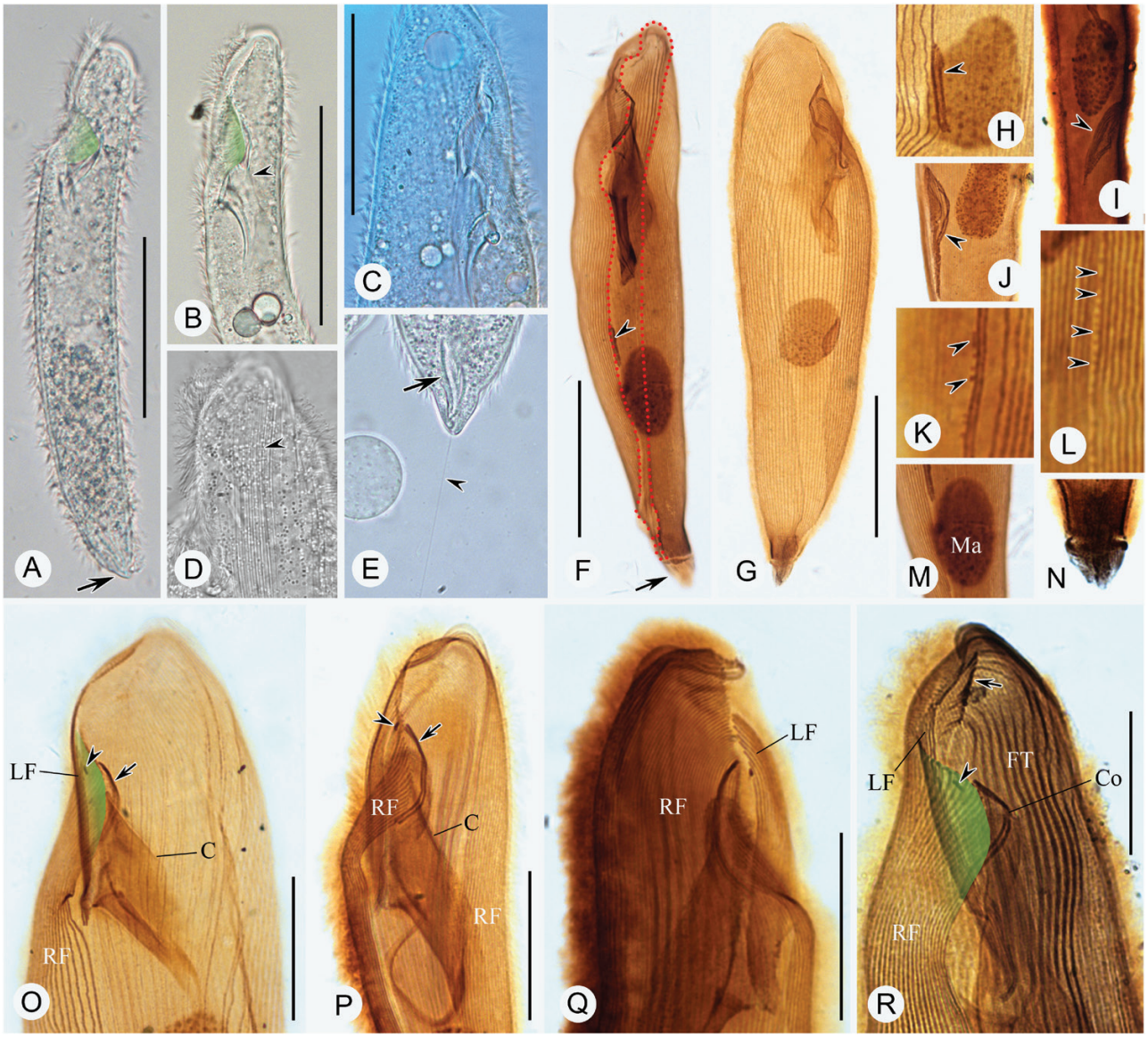

Figure 2. Photomicrographs of *Kyaroikeus paracetarius* from life (A–E) and after protargol impregnation (F–R). A, ventral view of a representative individual; the green region is the lip-like structure on the right side of oral cavity. B, ventral view of the anterior, to show the oral area, with the arrowhead indicating the cytopharynx. C, enlargement of the anterior of the cell. D, anterior of the cell, with the arrowhead indicating the non-ciliated stripe. E, posterior of the cell, with the arrow indicating the podite and arrowhead indicating the attachment thread. F, G. ventral and dorsal views of the infraciliature, with the arrowhead indicating the kinetofragments, the arrow indicating the podite, and the red dots outlining the non-ciliated area. H–J, mid-ventral region of several specimen with different shapes and number of kinetofragments, normal individual with four lines (H), individuals in early stage of fission with more lines (I, J). K, L, equatorial fragment (arrowheads), next to the middle part of the rightmost right kinety. M, the heteromeric macronucleus. N, the podite. O, P, enlargement of the oral region, with the arrows indicating the circumoral kineties and the arrowheads indicating the pre-oral kinety. Q, dorsal view of the anterior, showing the densely arranged right kineties (RK) and left kineties (LK). R, enlargement of the oral region, with the arrow indicating the pellicular fold, the arrowhead indicating the pre-oral kinety, and green region highlighting the lip-like structure. Abbreviations: C, cytostome; Co, circumoral kineties; FT, fibrous tracts; LF, left field; Ma, macronucleus; RF, right field. Scale bars = 60 μm (A–C, F, G) or 30 μm (O–R).

shape, extending with the same curve of the margin of the pellicular fold; each stratum contains several unequal-sized fragments, which are always two layered but with different numbers of microtubules (Fig. 5). Pellicular pores occur in the bases of grooves between the pellicular folds and are evenly separated,

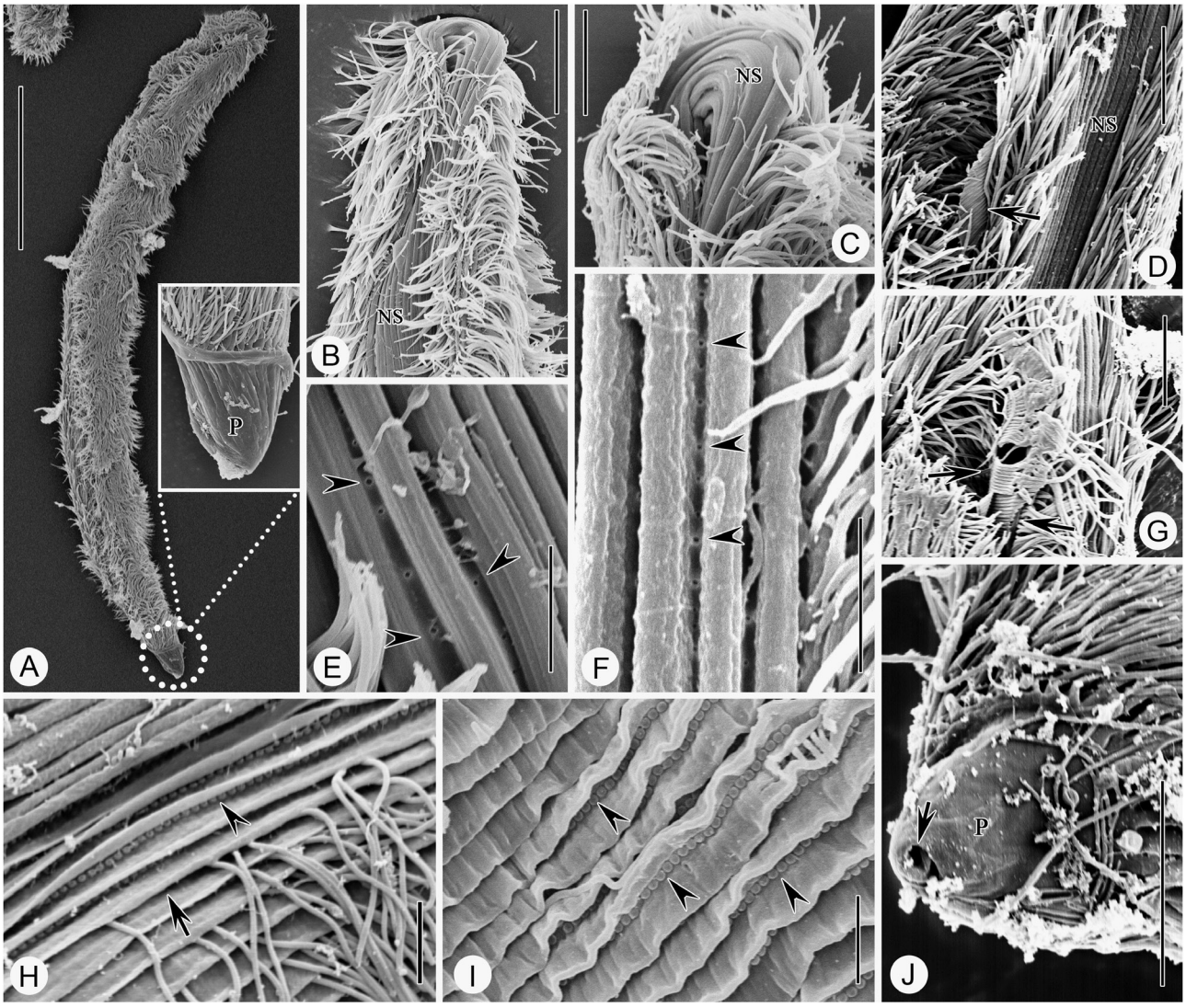

Figure 3. Scanning electron micrographs of *Kyaroikeus paracetarius*. A, the general body shape and the podite in posterior end (white circle). B, C, anterior portion of cell, showing the pellicular fold in the non-ciliated stripe, which hooks over the anterior end. D, G, oral area, with arrows indicating the circumoral kineties observed in different individuals. E, F, the non-ciliated stripe, with the arrowheads indicating the pellicular pores, which occur in the grooves between the pellicular folds. H, I, a de-ciliated specimen, showing the densely arranged kinetosomes (arrowheads) of ciliary rows and the pellicular ridges (arrow) in the right field of cell. J, the podite, indicating the secretion pore (arrow). Abbreviations: NS, non-ciliated stripe; P, podite. Scale bars = 50 μm (A), 10 μm (B), 5 μm (C, D, G, J) or 2 μm (E, F, H, I).

as revealed by SEM (Fig. 3E, F). In TEM, sacs (< 1 μm at their widest) regularly occur beneath the pellicle of each groove, some of which contain materials and even open toward the outside (Fig. 4F–I). There are often rich cytoplasmic vesicles containing granular material beneath the folds and near the secretory sacs (Figs 4I, 5). These results suggest a secretory system composed of the cytoplasmic vesicles, sacs and pellicular pores (Fig. 5). Mitochondria occur mainly in the cytoplasm of the cortex area (Fig. 4C, G). Cytoplasm also contains food vacuoles encasing various food granules of different electron-density (Fig. 4A).

PLANILAMIA MA *ET AL.*, 2006

PLANILAMINA OVATA MA *ET AL.*, 2006

(FIGS 6, 7; TABLE 1)

Improved diagnosis: Cell size 35–80 × 30–50 μm *in vivo*; laterally flattened, discoid or ovate in side

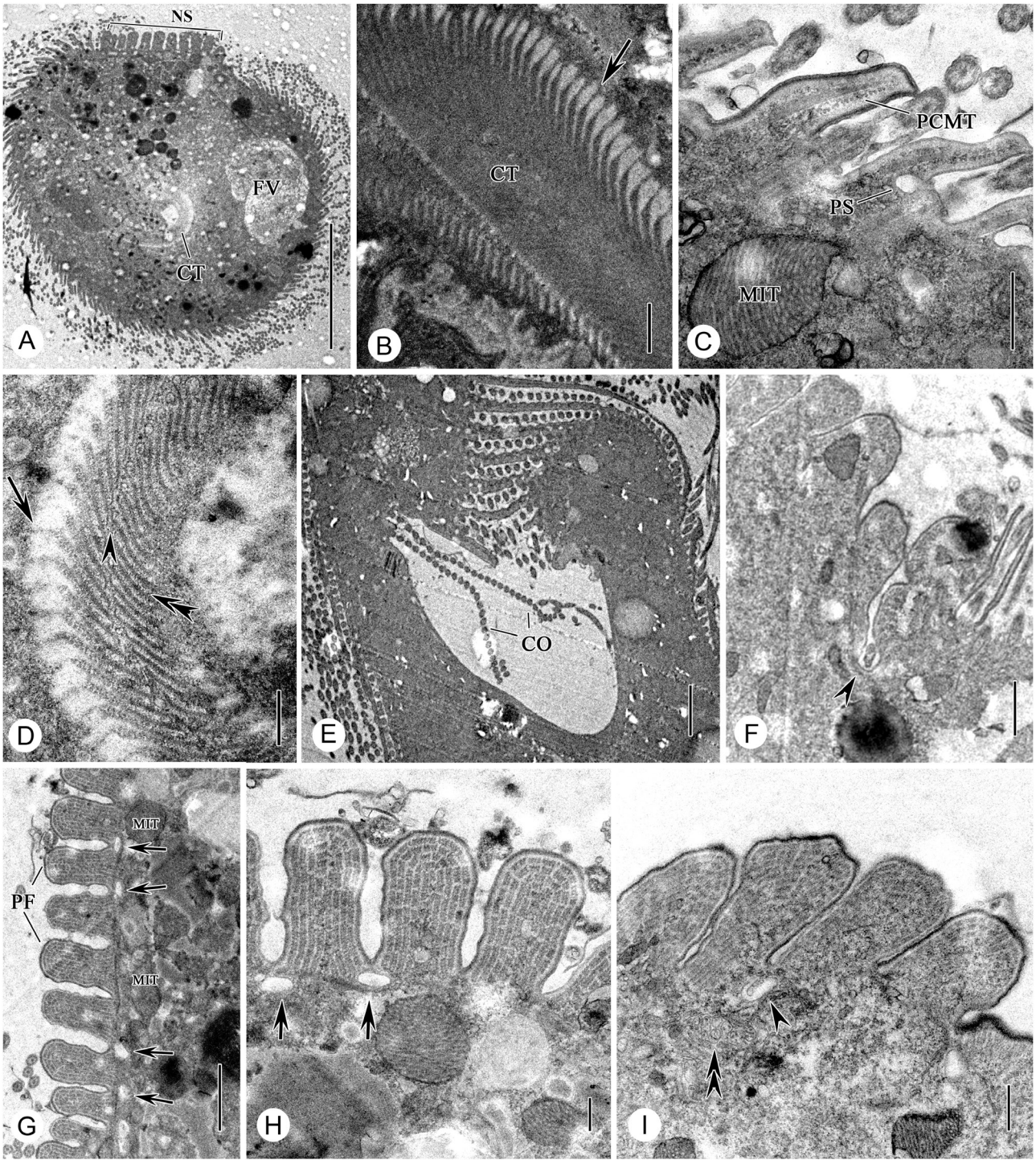

Figure 4. Transmission electron micrographs of *Kyaroikeus paracetarius*. A, cross-section showing the non-ciliated stripe, ciliated area (the surface part other than NF), cytopharyngeal tube and a food vacuole. B, D, details of cytopharyngeal tube, which is a flat vesicle. The arrows indicate the microtubule sheets with thinner ends, the double arrowhead indicates one of even thickness and the arrowhead indicates the narrow space of cytopharyngeal tube. C, the pellicular ridges, which were present between ciliary rows and supported by postciliary microtubules, and the parasomal sacs. E, the oral region, showing the two circumoral kineties that were composed of a single row of kinetosomes. F–I, the pellicular folds in the non-ciliated stripe, arrows indicate the sacs regularly occurred beneath the pellicle of each groove, arrowheads mark the sacs that

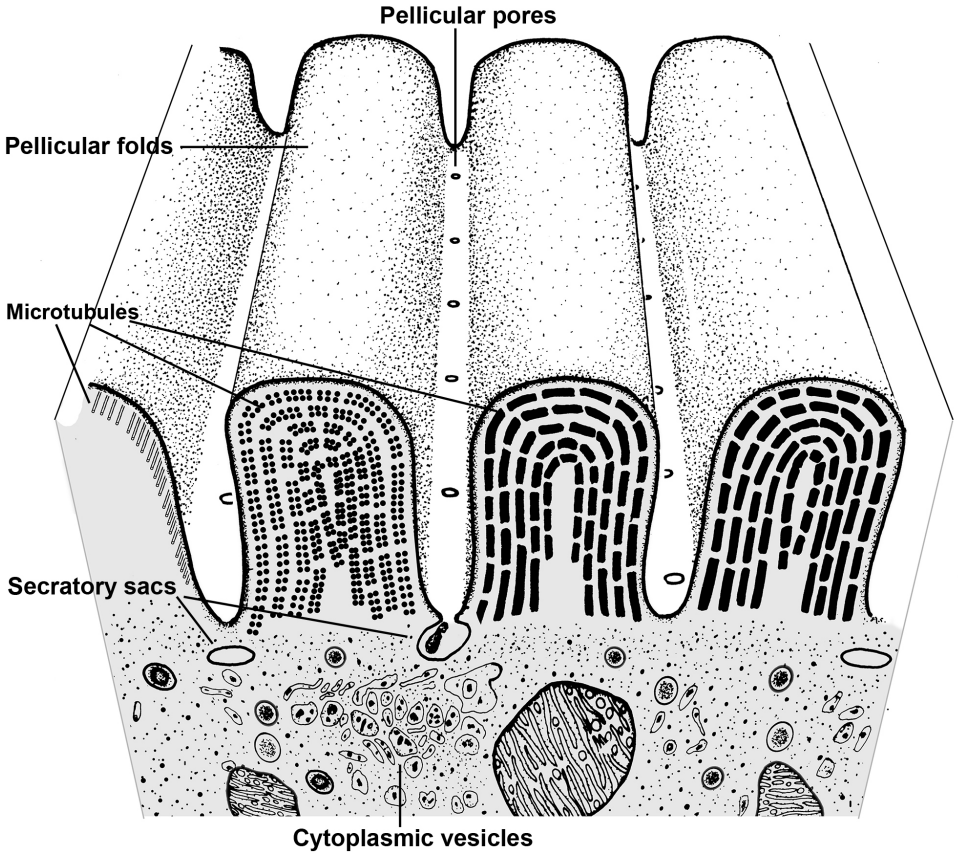

Figure 5. The cortex of the non-ciliated stripe of *Kyaroikeus paracetarius*, showing the arrangement of microtubules and a proposed material secretion system containing cytoplasmic vesicles, sacs and pellicular pores.

view; deep oral cavity composed of a pre-oral kinety (rarely two), two circumoral kineties and seven to 13 infundibular kineties; no nematodesmal rods; 38–58 right kineties, three to four left kineties; four kinetofragments located in the left ahead of the podite; macronucleus ovoid; one contractile vacuole adjacent to cytostome.

Host: Delphinapterus leucas (beluga whale).

Voucher material: Four slides with protargol-stained specimens (indicated with a black circle of ink on each coverslip) have been deposited in the collection of Ningbo University (registration numbers: LJ-II-20170502-01, 02, 03 and 04).

General morphology and ciliary pattern of Ningbo population: The cell size is 55–80 × 40–50 μm *in vivo* and 50–80 × 32–47 μm after protargol staining. The body is laterally flattened in shape with a length–width ratio of about 3:2 in lateral view (Figs 6A, 7A). From lateral view, the cell is discoid or ovate in outline; the anterior end is slightly pointed and the posterior margin is broadly rounded (Fig. 6A, C). The dorsal margin of the ciliated right region is sculptured by a C-shaped band (or groove) (Fig. 7A, M). This band extends from the cell apex to the posterior end. Some long bands (23 out of 35 individuals observed) curve around the posterior end and anteriorly on to the left of the podite. This structure is visible as a deep groove *in vivo* and as an argentophilic band (AB) in protargol-impregnated specimens (Fig. 6D, E). The left surface is not regular in shape (Figs 6B, 7B). The oral cavity is broad and located at the anterior quarter of the cell. The cytostome is located posteriorly in the oral cavity (Figs 6F, 7G, I, M). The cytoplasm is colourless,

contained materials or connected with the outside, double-arrowhead marks the rich cytoplasmic vesicles in the cytoplasm beneath the folds and near the sacs. Abbreviations: Co, circumoral kineties; CT, cytopharyngeal tube; FV, food vacuole; MIT, mitochondria; NS, non-ciliated stripe; PCMT, postciliary microtubules; PS, parasomal sacs; Scale bars = 10 μm (A), 0.5 μm (B–D, H, I) or 2 μm (E, G), 1 μm (F).

Table 1. Morphometric data of *Kyaroikeus paracetarius* (upper line) and *Planilamina ovata* (lower line) based on Protargol-stained specimens

character	Max	Mix	Mean	Median	SD	SE	CV	*N*
Body length (μm)	364.0	150.0	210.3	203.5	47.5	9.3	22.6	26
	80.0	50.0	61.6	61.0	7.7	1.5	12.4	26
Body width (μm)	77.0	34.0	48.4	47.0	10.5	2.1	21.7	26
	47.0	32.0	38.2	37.5	4.2	0.8	11.1	26
Macronucleus, length (μm)	75.0	22.0	37.8	34.0	12.0	2.4	31.8	26
	27.0	12.0	18.1	18.0	3.3	0.7	18.3	26
Macronucleus, width (μm)	32.0	13.0	19.5	19.0	4.2	0.8	21.6	26
	20.0	9.0	13.8	13.5	3.4	0.7	24.8	26
Podite, length (μm)	13.0	6.0	10.0	10.5	2.0	0.4	20.0	26
	—	—	—	—	—	—	—	—
Podite, width (μm)	11.0	5.0	8.6	9.0	1.7	0.3	20.4	26
	8.0	3.0	5.6	6.0	1.1	0.2	20.4	26
Cell apex to proximal end of left ciliary field, distance (μm)	41.0	6.0	17.5	16.0	7.5	1.5	42.7	26
	14.0	3.0	8.9	9.5	2.9	0.6	32.7	26
Cell apex to distal end of left ciliary field, distance (μm)	77.0	24.0	63.9	67.0	11.5	2.3	18.0	26
	—	—	—	—	—	—	—	—
Left field, length (μm)	—	—	—	—	—	—	—	—
	35.0	17.0	25.2	24.5	5.0	1.0	19.9	26
Circumoral arch, length (μm)	—	—	—	—	—	—	—	—
	13.0	6.0	8.1	8.0	1.6	0.3	19.5	26
Circumoral arch, width (μm)	—	—	—	—	—	—	—	—
	7.0	3.0	4.7	4.5	1.1	0.2	23.2	26
Cell apex to proximal end of pre-oral kinety, distance (μm)	37.0	22.0	30.4	31.0	4.8	0.9	15.8	26
	18.0	11.0	13.9	14.0	1.8	0.3	12.6	26
Cell apex to proximal end of circumoral kineties, distance (μm)	38.0	20.0	29.9	31.0	5.2	1.0	17.6	26
	17.0	10.0	13.0	13.0	1.6	0.3	12.6	26
Cell apex to distal end of circumoral kineties, distance (μm)	58.0	34.0	48.6	50.5	7.0	1.4	14.5	26
	23.0	16.0	19.1	19.0	1.8	0.4	9.5	26
Cell apex to proximal end of kinetofragments, distance (μm)	174.0	77.0	117.4	119.5	22.8	4.5	19.4	26
	48.0	28.0	37.7	37.0	4.5	0.9	11.8	26
Cell apex to distal end of kinetofragments, distance (μm)	206.0	92.0	136.2	134.5	27.0	5.3	19.8	26
	—	—	—	—	—	—	—	—
Kinetofragments, length (μm)	—	—	—	—	—	—	—	—
	15.0	6.0	9.6	9.0	2.2	0.4	23.4	26
Cell apex to tip of podite, distance (μm)	—	—	—	—	—	—	—	—
	60.0	39.0	47.1	46.0	5.3	1.0	11.2	26
Cell apex to proximal end of cytopharynx, distance (μm)	44.0	24.0	35.1	36.0	5.7	1.1	16.2	26
	—	—	—	—	—	—	—	—
Cell apex to posterior curvature of cytopharynx, distance (μm)	—	—	—	—	—	—	—	—
	34.0	25.0	29.1	28.0	2.2	0.4	7.5	26
Pre-oral kineties, number	1.0	1.0	1.0	1.0	0.0	0.0	0.0	26
	1.0	1.0	1.0	1.0	0.0	0.0	0.0	26
Circumoral kineties, number	2.0	2.0	2.0	2.0	0.0	0.0	0.0	26

Table 1. Continued

character	Max	Mix	Mean	Median	SD	SE	CV	*N*
	2.0	2.0	2.0	2.0	0.0	0.0	0.0	26
Infundibular kineties, number	—	—	—	—	—	—	—	—
	13.0	9.0	10.8	11.0	1.2	0.2	11.1	26
Somatic kineties, number	79.0	49.0	66.0	66.0	8.2	1.6	12.4	26
	61.0	45.0	51.5	51.0	3.8	0.7	7.3	26
Right field kineties, number	69.0	37.0	56.0	57.0	8.0	1.6	14.2	26
	58.0	41.0	48.0	47.5	3.7	0.7	7.8	26
Left field kineties, number	13.0	7.0	10.0	10.0	2.0	0.4	19.6	26
	4.0	3.0	3.5	3.5	0.5	0.1	14.6	26
Kinetofragments, number	4.0	4.0	4.0	4.0	0.0	0.0	0.0	26
	4.0	4.0	4.0	4.0	0.0	0.0	0.0	26
Fibrous bundles of non-ciliated surface, number	16.0	11.0	14.5	15.0	1.1	0.2	7.3	26
	—	—	—	—	—	—	—	—
Basal bodies in equatorial fragment, number	28.0	5.0	15.2	15.0	6.7	1.3	43.7	25
	—	—	—	—	—	—	—	—

Abbreviations: CV, coefficient of variation in %; Max, maximum; Mean, arithmetic mean; Min, minimum; *n*, number of specimens examined; SD, standard deviation; SE, standard error.

containing multiple food vacuoles consisting of unidentified amorphous material. The single contractile vacuole is up to 6 μm across and positioned at the left of mid-body in ventral view; contraction occurs with an interval of 20–30 s; the contractile vacuole pore is located between the second and third right kineties in mid-body (Fig. 6A, E).

The macronucleus is ovoid and heteromerous, located in mid-body (Figs 6F, 7M). The micronucleus is ellipsoid and adjacent to the macronucleus (Fig. 6D). The podite is broadly cone-shaped, situated in the posterior quarter of cell, about 4–6 μm in length and 3–8 μm across at the base (Figs 6A, E, 7A). Individuals are often attached to the substrate by the podite and rotate through viscous medium with the cilia beating in a regular pattern.

Cilia are about 8 μm long *in vivo*. The ciliature is shown in Figs 6E, F, 7F–M. Kinetosomes in somatic kineties are densely arranged. Somatic kineties are divided into three parts: right, left and kinetofragments. The right field comprises 41–58 kineties; the leftmost has 15–25 relatively short kineties, extending from the level of the oral field to the level of the podite; remaining kineties originate from the apex of the cell and extend posteriorly to the cell end and bend to the left (Fig. 6E). Three to four left kineties are located on the left of the oral cavity, originate from near the apex of the cell and terminate posteriorly at the level of the posterior margin of the cytostome, about two-fifths of the cell length (Figs 6E, 7G, H). Four short kinetofragments are located on the anterior-left of the podite and are often curved to the right. (Figs 6F, 7J, K, L). Equatorial fragment are not detected.

Oral ciliature is composed of a pre-oral kinety (seldom two), two parallel circumoral kineties and nine to 13 infundibular kineties (Fig 6F). Circumoral kineties are located on the anterior of the cytostome (Figs 6F, 7I). The pre-oral kinety is located on the anterior-left of the circumoral kineties, consisting of one or two closely set kinetosomes (Figs 6F, 7H). Infundibular kineties are positioned in an arc of circumoral kineties (Fig. 7H). The cytopharynx extends below mid-body and curves posteriorly; no nematodesmal rod is found (Figs 6F, 7G, M).

Molecular data and phylogenetic position (Figs 8–10)

The GenBank accession numbers, lengths and G+C contents of sequences (SSU and LSU rDNA, and ITS1-5.8S-ITS2) of *Kyaroikeus paracetarius* and *Planilamina ovata* from this study are provided in Table 2. The topologies of the BI and ML trees are almost identical, thus, only the ML tree is presented here, with support values from both of the algorithms indicated on branches.

SSU rDNA (Fig. 8): Planilamina ovata is sister to *Trochilia petrani* Dragesco, 1966 with low support values (ML/BI, 65%/0.80) and their clade then clustered with *Kyaroikeus paracetarius* with good support. The clade of *Trochilia/Kyaroikeus/Planilamina* in turn clusters with *Microxysma* Deroux, 1976 (ML/BI,

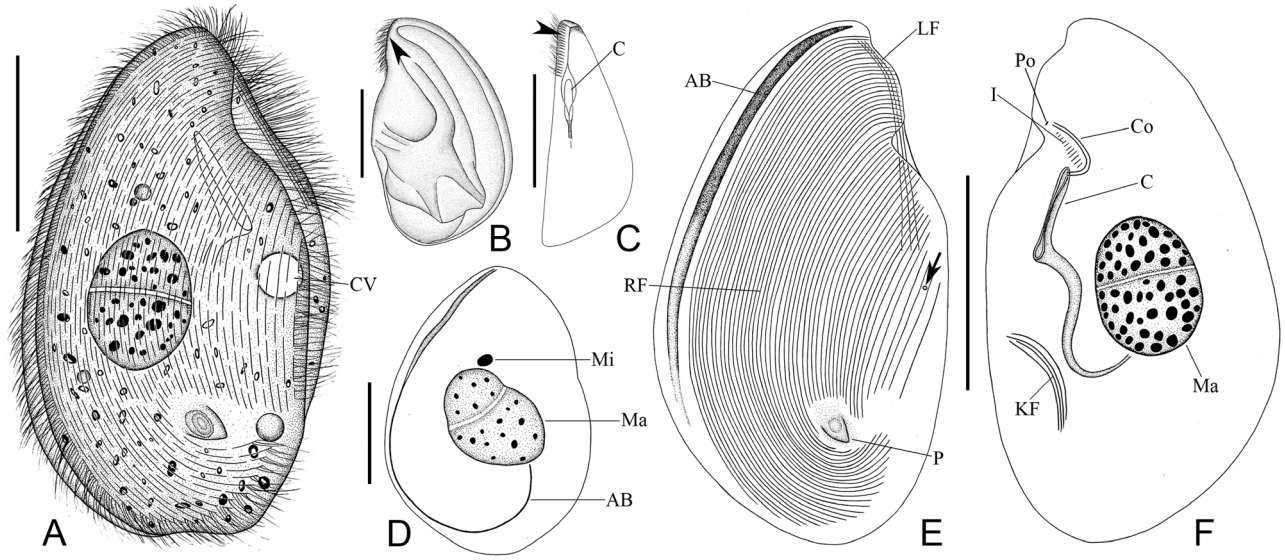

Figure 6. *Planilamina ovata* from life (A–C) and after protargol impregnation (D–F). A, right lateral view of a typical individual. B, left lateral view; arrowhead points to the anterior kineties of right field turning over onto dorsal side. C, ventral view; arrowhead points to the anterior kineties of right field turning over onto ventral side. D, right lateral view, showing the argentophilic band, macronucleus and micronucleus. E, right lateral view of ciliature; arrow indicates the contractile vacuole pore. F, left lateral view, showing the oral region, kinetofragments and macronucleus. Abbreviations: AB, argentophilic band; C, cytopharynx; Co, circumoral kineties; CV, contractile vacuole; I, infundibular kineties; KF, kinetofragments; LF, left field; Ma, macronucleus; Mi, micronucleus; P, podite; Po, pre-oral kineties; RF, right field. Scale bars = 25 μm.

80%/1.00) and then with the core of Dysteriidae species represented by *Dysteria* Huxley, 1857, *Mirodysteria* Kahl, 1933 and *Spirodysteria* Gong *et al.*, 2007, with moderate support values (ML/BI, 78%/0.98).

ITS1-5.8S-ITS2 (Fig. 9): Planilamina ovata clusters with *Kyaroikeus paracetarius* (ML/BI, 67%/0.82), forming a clade with *Dysteria derouxi* Gong & Song, 2004 (ML/BI, 88%/0.97).

LSU rDNA (Fig. 9): Kyaroikeus paracetarius clusters with *Planilamina ovata* with good support, and then this branch forms a clade with *Dysteria derouxi* with good support.

Concatenated genes (Fig. 10): The phylogenetic tree based on the concatenated dataset is different from the SSU rDNA tree; i.e. *Kyaroikeus paracetarius*, *Planilamina ovata* and *Trochilia petrani* group into a clade with 100% bootstrap support in the ML tree, but are not resolved by BI. The families Chilodonellidae and Lynchellidae are located in different positions: Lynchellidae is closer to Chlamydodontidae in the concatenated gene tree, while in the SSU rDNA tree Chilodonellidae is closer to Chlamydodontidae, and Lynchellidae is in a peripheral position.

DISCUSSION

As indicated in the Material and methods, the beluga whale was maintained in a closed, carefully controlled environment. It is unlikely that the ciliates arrived through contamination of the system. Rather, as the beluga whale was born in the wild, and the ciliates were found even when it was healthy, we presume that there are natural, low-level populations of ciliates in most whales that only become abundant when the whale is ill. Reports of ciliates from the respiratory tracts of other whales support this (Ma *et al.*, 2006; McFee & Lipscomb, 2009; Lair *et al.*, 2016).

Several studies suggested that ciliates infesting whale respiratory tracts belong to two genera, *Kyaroikeus* and *Planilamina*, within which species are morphologically adapted to a parasitic life (Sniezek *et al.*, 1995; Ma *et al.*, 2006). However, because of the lack of molecular and morphological information, a poor understanding remains of the phylogenetic positions, evolutionary origin and adaptive modifications of these species. Here, we apply state-of-the-art approaches (Warren *et al.*, 2017) to recognize and characterize two species found in an infected beluga whale: *K. paracetarius* and *P. ovata*. Considering their exceptionally high abundance when the host was ill, we consider these species to be parasites. Based on

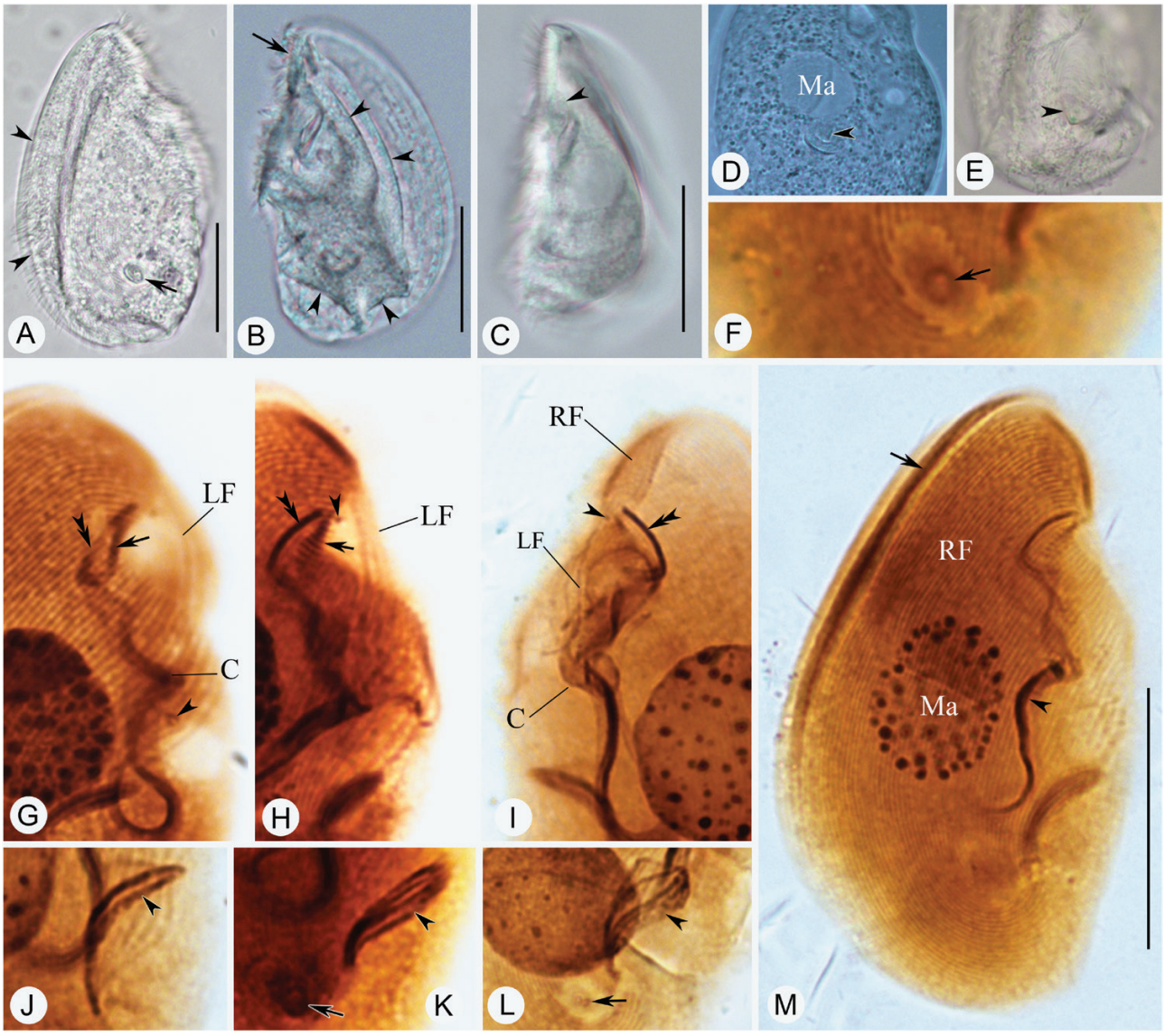

Figure 7. *Planilamina ovata* from life (A–E) and after protargol impregnation (F–M). A. right lateral view of a representative individual; arrow indicates the podite and arrowheads indicate the C-shaped bright groove B, left lateral view; arrow points to the anterior kineties of right field turning over to dorsal side and arrowheads show the short grooves on surface. C, ventral view; arrowhead indicates oral region. D, E, arrowheads indicate the podite. F, showing the podite (arrow). G, showing the oral region; arrow indicates infundibular kineties, double arrowheads indicate circumoral kineties, and arrowhead indicates the contractile vacuole pore. H, I, showing the oral region; arrow indicates infundibular kineties, arrowheads indicate pre-oral kineties, and double arrowheads indicate circumoral kineties. J–L, specimen in different shape and numbers of kinetofragments (arrowheads); arrows indicate the podite. M, right lateral view of ciliature; arrow indicates argentophilic band and arrowhead indicates cytopharynx. Abbreviations: C, cytopharynx; LF, left field; Ma, macronucleus; RF, right field. Scale bars = 25 μm (A–C, M).

our phylogenetic and morphological analyses, we suggest revisions to the systematic positions of the two parasitic genera and speculate how they may have invaded the host and their morphological adaptations to reside in the blow-holes of beluga whales.

Beyond these fundamental aspects of phylogeny and adaptation, we suggest that a good appreciation of the biology of this potential pathogen may be useful to understand disease in whales. Information on phylogeny and evolutionary origin can provide

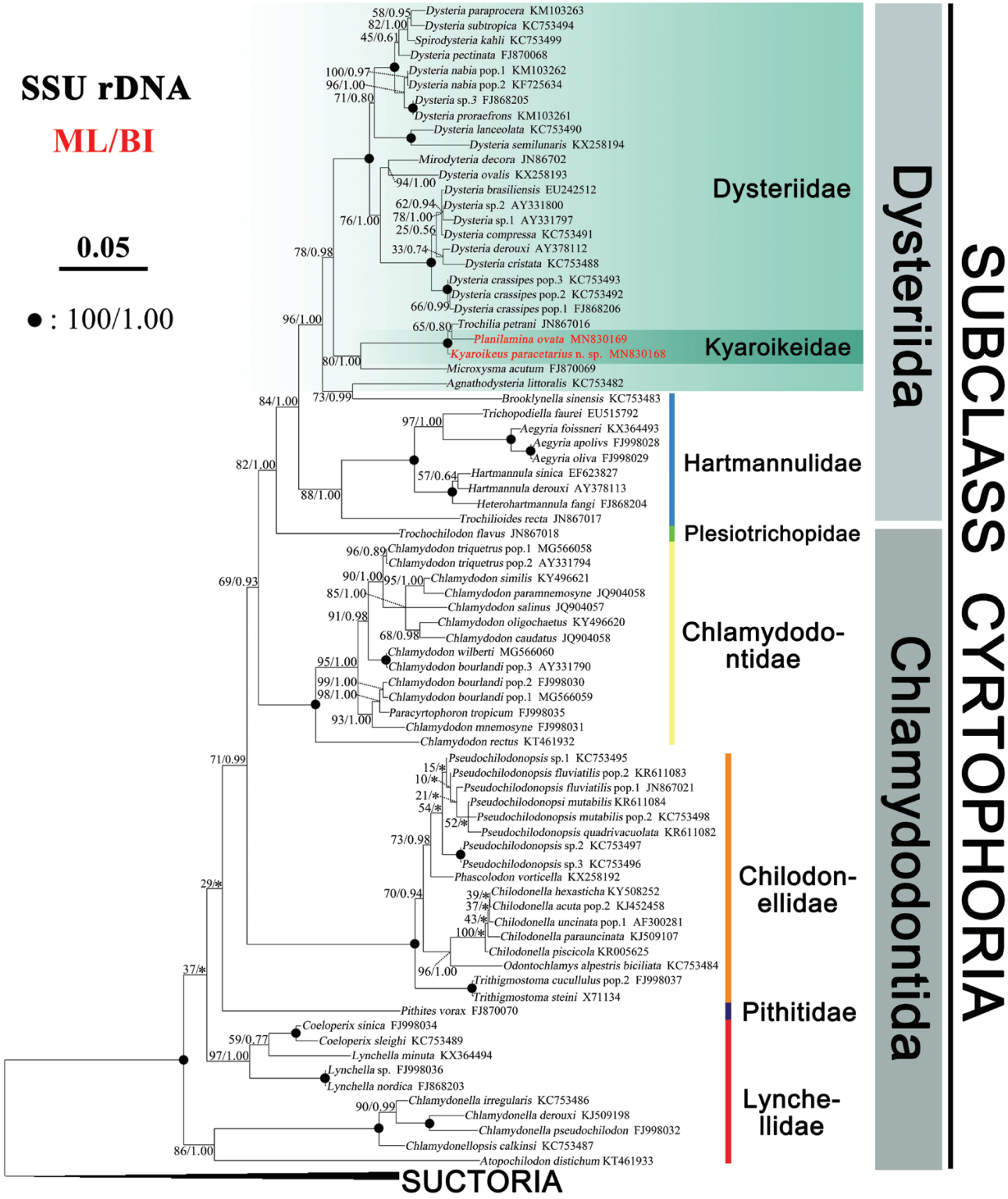

Figure 8. Phylogenetic tree inferred from SSU rDNA sequences, revealing the position of *Kyaroikeus paracetarius* and *Planilamina ovata* (red font). Numbers near branches represent posterior probabilities for BI and bootstrap values for ML. Asterisks indicate topologies that differ between the ML and BI phylogenies. Fully supported (100/1.00) branches are marked with solid circles. The scale bar corresponds to five substitutions per 100 nucleotide sites.

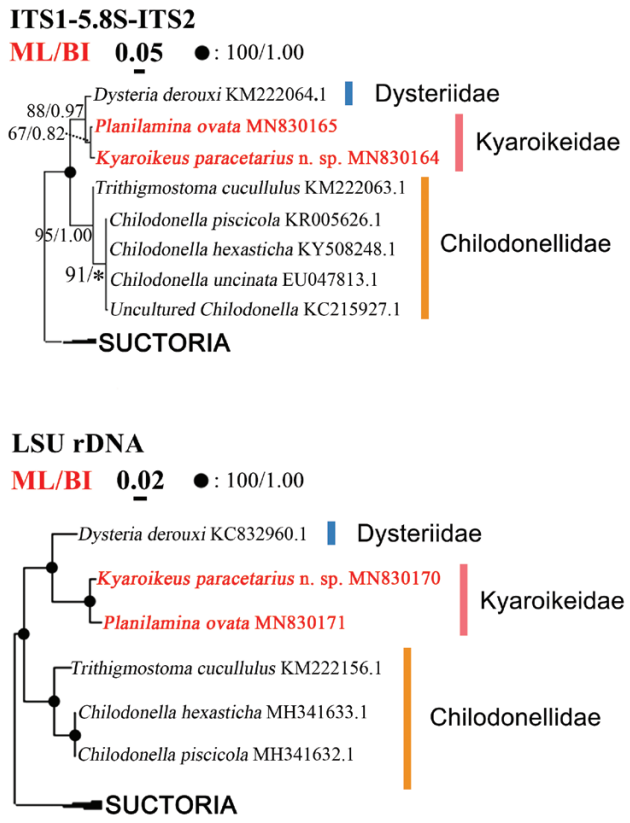

Figure 9. Phylogenetic trees inferred from ITS1-5.8S-ITS2 and LSU rDNA sequences, revealing the position of *Kyaroikeus paracetarius* and *Planilamina ovata* (red font). Numbers near branches represent posterior probabilities for BI and bootstrap values for ML. Asterisks indicate topologies that differ between the ML and BI phylogenies. Fully supported (100/1.00) branches are marked with solid circles. The scale bar corresponds to five substitutions per 100 nucleotide sites.

insights into other potential pathogens and adaptive features associated with specific lineages. Existing knowledge of near phylogenetic neighbours may also offer insights into key functions of pathogens. Clearly, also understanding how pathogens have adapted to a parasitic lifestyle allows researchers to consider how they act and how they may be prevented from acting. We hope, therefore, that our work will be wide-reaching in its impact.

Establishment of the new *Kyaroikeus* species

Sniezek *et al.* (1995) established the genus *Kyaroikeus* and described its type species *K. cetarius*. The main features of our isolate fit the diagnosis of the genus *Kyaroikeus*, supporting the genetic placement of the new species. However, our organism differs from its only congener *K. cetarius* in two key attributes: a larger number of right somatic kineties [37–69 (arithmetic mean 66) vs. 44–51 (arithmetic mean 48) in *K. cetarius*] and, critically, the number of left kineties, considered stable in cyrtophorid ciliates [our isolate has seven to 13 left kineties (arithmetic mean ten), while *K. cetarius* has only four]. Although there is variation in the number of right and left kineties in *K. paracetarius*, there is no clear correlation between these, nor did they appear to be correlated with cell size (Supporting Information, Fig. S3), suggesting that the variation is random Accordingly, we establish it as a new species: *K. paracetarius*.

Comments on *Planilamina ovata*

Planilamina ovata was first collected from Atlantic bottlenose dolphins and a false killer whale in the USA, and was described by Ma *et al.* (2006) using the protargol staining method. The Ningbo population closely matches the original description in body shape, living and stained morphological features, except for some minor differences: the Ningbo population has a larger cell size *in vivo* (50–80 × 32–47 μm vs. 28–65 × 20–43 μm) and has a wider range number of right kineties (41–58 vs. 41–51). These are minor differences, and the ranges overlap, so we conclude that our identification of the Ningbo population is correct.

Parasites arose from a Dysteriidae ancestor

Sniezek & Coats (1996) established the family Kyaroikeidae with *Kyaroikeus* as the type genus, placed this family in the order Cyrtophorida and, according to their morphogenesis, suggested this family to be closely related to the family Dysteriidae, which is currently composed only of free-living species. Later, Ma *et al.* (2006) erected the parasitic genus *Planilamina* and assigned it to Kyaroikeidae. Our SSU rDNA-based phylogenetic results support that the two genera belong to the subclass Cyrtophoria (Fig. 8), and the general topologies of the subclass match the results of others (e.g. Gao *et al.*, 2012; Chen *et al.*, 2016; Qu *et al.*, 2017). However, addition of our new gene sequences questions the validity of the Kyaroikeidae, because the clade represented by this family includes both parasitic and free-living genera and falls within Dysteriidae (Fig. 8). This molecular clustering is also reflected by morphological characteristics; i.e. the kyaroikeids and dysteriids share a similar ciliary pattern in that they both include highly degenerated left kineties in the front-left of the cell and short post-oral kineties in mid-body (Figs 1A, 6A; Lynn, 2008).

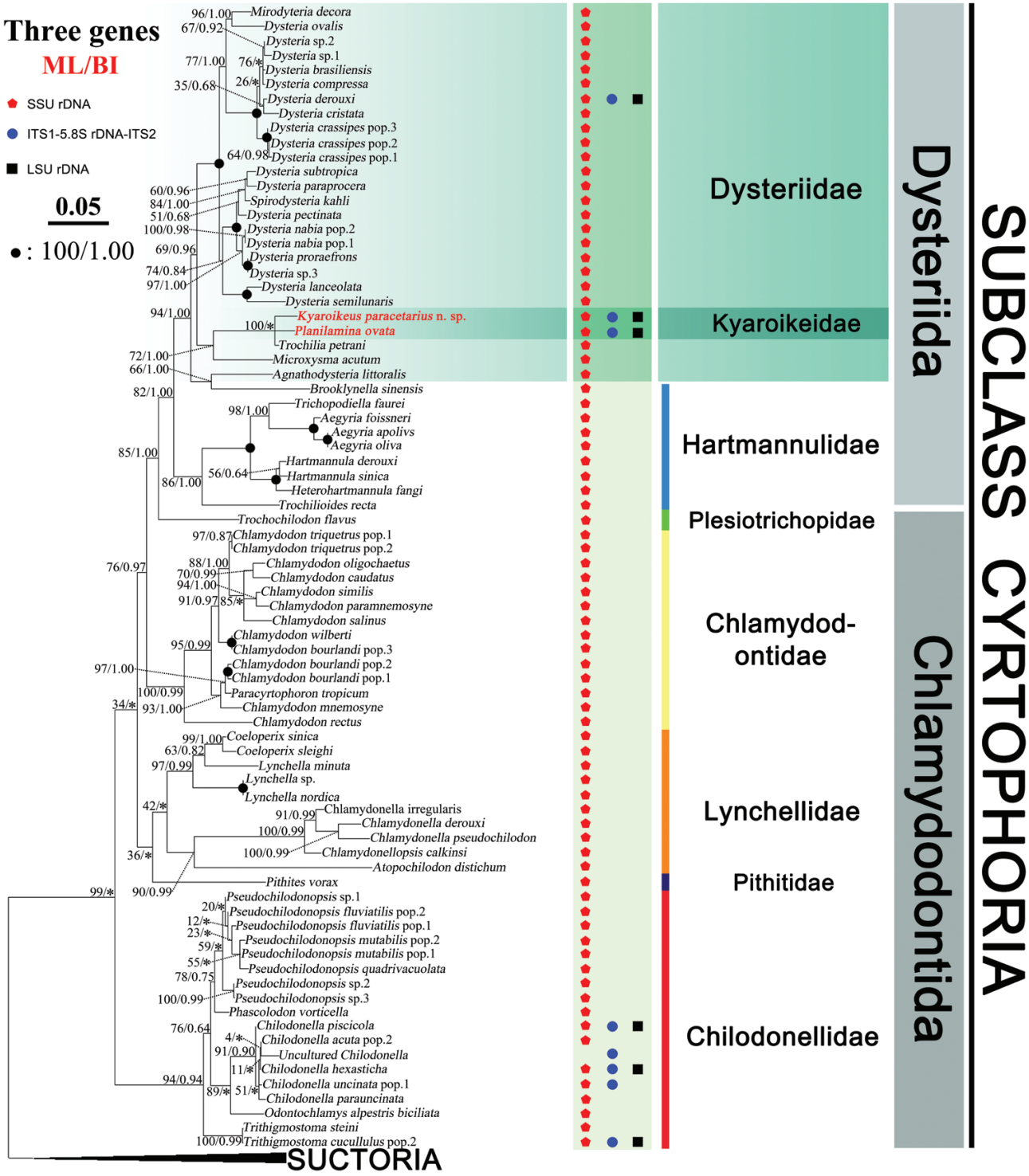

Figure 10. Phylogenetic tree inferred from the concatenated genes (SSU rDNA, ITS1-5.8S-ITS2, LSU rDNA), revealing the position of *Kyaroikeus paracetarius* and *Planilamina ovata* (red font). Numbers near branches represent posterior probabilities for BI and bootstrap values for ML. Asterisks indicate topologies that differ between the ML and BI phylogenies. Fully supported (100/1.00) branches are marked with solid circles. The scale bar corresponds to five substitutions per 100 nucleotide sites.

Table 2. Accession numbers, lengths and G+C contents of sequences provided in present work

Species		*K. paracetarius*	*P. ovata*
SSU rDNA	Accession number	MN830168	MN830169
	Length	1677 bp	1552 bp
	GC content	43.71%	44.91%
ITS1-5.8S-ITS2	Accession number	MN830164	MN830165
	Length	421bp	398bp
	GC content	41.81%	41.96%
LSU rDNA	Accession number	MN830170	MN830171
	Length	1739bp	1772bp
	GC content	44.85%	44.70%

The two parasitic genera, representing the current Kyaroikeidae, do exhibit unique features (i.e. a large number of right kineties, large ciliated regions and dense cilia; Figs 1H, I, 6E). However, the free-living genus *Trochilia*, which clusters with the two parasitic ciliates, is morphologically more like other free-living members of the Dysteriidae (see fig. 4K in Liu *et al.*, 2017). We suggest that the unique structures of the parasites (i.e. dense cilia, pellicular fold contained five to six layers, prominent oral cavity and pellicular pores) are convergent and arose through adaptation to their novel environment (see next section). Thus, we propose that, as a family, Kyaroikeidae is superfluous and suggest that, for the time being, it should be treated as a subfamily of Dysteriidae.

Regardless of the formal position of Kyaroikeidae, our phylogenetic analysis clearly indicates that the parasitic genera *Planilamina* and *Kyaroikeus* evolved from a free-living Dysteriidae-like ancestor. Furthermore, the close association of the free-living genus *Trochilia* to the parasitic genus *Planilamina* (Fig. 8) implies that parasitism may have arisen more than once.

The free-living Dysteriidae tend to occupy periphytic environments, including sediments, sea ice and associations with marine algae (Petz *et al.*, 1995; Song & Wilbert, 2000; Meng *et al.*, 2018). Marine mammals and, specifically, beluga whales will roll in sediments and rub against hard surfaces to remove dead skin and ectoparasites (Smith *et al.*, 1992). This may have allowed invasion of free-living Dysteriidae into their respiratory system, where they evolved to live permanently. Undoubtedly, when more parasitic and free-living taxa in these clades are recognized, our predictions may be more rigorously evaluated.

Morphological modifications for a parasitic life

Kyaroikeus paracetarius and *Planilamina ovata* appear to be obligatory parasites, as they could not live freely in water (see Methods). We suggest that they have morphologically adapted to this life by evolving structures that: (1) increase movement through viscous mucus; (2) improve ingestion of cellular material; and (3) adhere to flocs of mucus and facilitate food uptake. We outline these below and suggest they are worthy of further investigation.

Increased movement through viscous mucus: The free-living dysteriid species have few, fragmented right kineties (at most 13 rows in Dysteriidae spp. and only four in *Trochilia* spp.), and these are constrained in a narrow, ventral groove with sparsely distributed cilia and weak microtubule structure (Qu *et al.*, 2015). In contrast, the two parasitic species have many non-fragmented right kineties that occupy a substantial part of the cell surface (Figs 1H–J, 6E); they also are densely ciliated. We suggest that these modifications contribute to the motility of the organisms in viscous mucus. Moreover, the cortex of the dorsal surface is compressed into stripes and, under these pellicular folds, there is a unique microtubular structure (outlined below and described by Sniezek *et al.*, 1995). In several groups of ciliates, microtubules that run longitudinally under the pellicle allow cells to maintain and change cell shape (Lynn, 2008). Generally, there are only one or two layers and several bundles of these microtubules (Calvo *et al.*, 1986; Wirnsberger-Aescht *et al.*, 1989; Kurth & Bardele, 2001). However, in *K. paracetarius*, each pellicular fold contains five to six layers and multiple bundles (Figs 4H, 5), suggesting a greater role in movement, possibly allowing cells to penetrate the mucus. (Supporting information, Supplementary Video S1).

Improved ingestion of cellular material: Compared to the free-living dysteriids, the two parasitic genera have a pronounced oral cavity. The oral region reflects functional diversity among ciliates (Eisler, 1992). For members of the free-living dysteriids, their oral region is prominent with strong nematodesmal rods, allowing

them to capture particulate food (Foissner *et al.*, 1991; Qu *et al.*, 2015). In contrast, the two parasitic species have densely arranged cilia near the oral area that are likely used to transport large volumes of liquid, moving large food particles (exfoliated epithelial cells) towards the cytostome into their deep oral cavity (Figs 1E, F, 6A).

Adhering to mucus and improved food uptake: Pellicular pores that occur in the pellicle of sessile peritrich ciliates (e.g. Lom & Corliss, 1968; Finley *et al.*, 1972) are considered to be sites of mucus material secretion, lorica-formation and stalk-production (Bauer-Nebelsick *et al.*, 1996; Lynn, 2008). To our knowledge, such pores are not reported in free-living dysteriids. However, they are also found in the non-ciliated area and the podite of an ectoparasitic ciliate (*Brooklynella hostilis* Lom & Nigrelli, 1970) of marine fishes (Lom & Corliss, 1971). Similar structures occur in *Cryptocaryon irritans* Brown, 1951, a parasitic ciliate causing white spot disease of marine fishes, where pellicular openings are connected to small vesicles and may serve in enzyme excretion or food uptake (Matthews *et al.*, 1993). We observed pellicular pores in *K. paracetarius* (Figs 3E, F, 4H, 5) and suggest that they may function in secretion of mucus material (for adhesion) or secretion of enzymes (aiding in feeding).

CONCLUSION

In this study, we provide an evaluation of the occurrence and abundance of two ciliates that appear to be parasites (but may, admittedly, be opportunistic endocommensals) within the respiratory tract of a beluga whale. Our efforts to culture the ciliates were not successful. We suggest that continued work explores the protozoa in the mucus of whales, evaluating changes in abundance and making further efforts to culture taxa to reveal their life cycles. Furthermore, now that we have provided substantial molecular data for these taxa, we encourage the development of barcoding approaches (Zhao *et al.*, 2018) to allow rapid assessment of these taxa on a wider scale.

CONFLICT OF INTEREST

The authors declare that they have no competing interests.

ACKNOWLEDGEMENTS

This work was supported by the National Natural Science Foundation of China (grant numbers 31970398, 41876151), the Technology Innovation Team of Ningbo city (grant number 2015C110018) and the K. C. Wong Magna Fund in Ningbo University.

REFERENCES

Bauer-Nebelsick M, **Bardele CF**, **Ott JA. 1996.** Electron microscopic studies on *Zoothamnium niveum* (Hemprich & Ehrenberg, 1831) Ehrenberg, 1838 (Oligohymenophora, Peritrichida), a ciliate with ectosymbiotic, chemoautotrophic bacteria. *European Journal of Protistology* **32:** 202–215.

Calvo P, **Torres A**, **Fedriani C**, **Rios RM**, **Silva JP. 1986.** Ultrastructure chez *Histriculus similis* (Cilié hypotriche). *Acta Protozoologica* **25:** 23–32.

Chen X, **Pan H**, **Huang J**, **Warren A**, **Al-Farraj SA**, **Gao S. 2016.** New considerations on the phylogeny of cyrtophorian ciliates (Protozoa, Ciliophora): expanded sampling to understand their evolutionary relationships. *Zoologica Scripta* **45:** 334–348.

Choi YK, **Kang MS**, **Sohn HR**, **Kim DY. 2003.** Disseminated ciliated protozoan infection in a Pacific dolphin (*Tursiops gill*). *Veterinary Record* **153:** 714–715.

Eisler K. 1992. Somatic kineties or paroral membrane: which came first in ciliate evolution? *BioSystems* **26:** 239–254.

Finley HE, **Ranganathan VS**, **Small EB. 1972.** Examination of the peritrich ciliate *Telotrochidium* by scanning electron microscopy. *Transactions of the American Microscopical Society* **91:** 492–501.

Foissner W, **Blatterer H**, **Berger H**, **Kohmann F. 1991.** Taxonomische und ökologische Revision der Ciliaten des Saprobiensystems – Band I: Cyrtophorida, Oligotrichida, Hypotrichia, Colpodea. *Informationsberichte des Bayer. Landesamtes für Wasserwirtschaft* **1/91**: 1–478.

Gao S, **Huang J**, **Li J**, **Song W. 2012.** Molecular phylogeny of the cyrtophorid ciliates (Protozoa, Ciliophora, Phyllopharyngea). *PLoS One* **7:** e33198.

Gao F, **Warren A**, **Zhang Q**, **Gong J**, **Miao M**, **Sun P**, **Xu D**, **Huang J**, **Yi Z**, **Song W. 2016.** The all-data-based evolutionary hypothesis of ciliated protists with a revised classification of the phylum Ciliophora (Eukaryota, Alveolata). *Scientific Reports* **6:** 24874.

Gulland MD, **Dierauf A**, **Whitman L. 2018.** Protozoan parasites of marine mammals. In: Miller M, ed. *CRC handbook of marine mammal medicine*, *3nd edn*. Boca Raton: CRC Press, 425–470.

Hall TA. 1999. BioEdit: a user-friendly biological sequence alignment editor and analysis program for Windows 95/98/NT. *Nucleic Acids Symposium Series* **41:** 95–98.

Hermosilla C, **Silva LMR**, **Prieto R**, **Kleinertz S**, **Taubert A**, **Silva MA. 2015.** Endo- and ectoparasites of large whales (Cetartiodactyla: Balaenopteridae, Physeteridae): overcoming difficulties in obtaining appropriate samples by non- and minimally-invasive methods. *International Journal for Parasitology: Parasites and Wildlife* **4:** 414–420.

Hermosilla C, **Silva LMR**, **Kleinertz S**, **Prieto R**, **Silva MA**, **Taubert A. 2016.** Endoparasite survey of free-swimming

baleen whales (*Balaenoptera musculus*, *B. physalus*, *B. borealis*) and sperm whales (*Physeter macrocephalus*) using non/minimally invasive methods. *Parasitology Research* **115:** 889–896.

Hu X, **Lin X**, **Song W. 2019.** *Ciliate atlas: species found in the South China Sea*. Beijing: Science Press.

Kurth T, **Bardele CF. 2001.** Fine structure of the cyrtophorid ciliate *Chlamydodon mnemosyne* Ehrenberg, 1837. *Acta Protozoologica* **40:** 33–48.

Lair S, **Measures LN**, **Martineau D. 2016.** Pathologic findings and trends in mortality in the beluga (*Delphinapterus leucas*) population of the St Lawrence Estuary, Quebec, Canada, from 1983 to 2012. *Veterinary Pathology* **53:** 22–36.

Liu W, **Jiang J**, **Xu Y**, **Pan X**, **Qu Z**, **Luo X**, **El-Serehy H**, **Warren A**, **Ma H**, **Pan H. 2017.** Diversity of free-living marine ciliates (Alveolata, Ciliophora): Faunal studies in coastal waters of China during the years 2011–2016. *European Journal of Protistology* **61:** 424–438.

Lom J, **Corliss JO. 1968.** Observations on the fine structure of two species of the peritrich ciliate genus *Scyphidia* and on their mode of attachment to their host. *Transactions of the American Microscopical Society* **87:** 493–509.

Lom J, **Corliss JO. 1971.** Morphogenesis and cortical ultrastructure of *Brooklynella hostilis*, a dysteriid ciliate ectoparasitic on marine fishes. *Journal of Protozoology* **18:** 261–281.

Lynn DH. 2008. *The ciliated Protozoa, characterization, classification, and guide to the literature*. Dordrecht: Springer.

Ma H, **Overstreet RM**, **Sniezek JH**, **Solangi M**, **Wayne Coats D. 2006.** Two new species of symbiotic ciliates from the respiratory tract of cetaceans with establishment of the new genus *Planilamina* n. gen. (Dysteriida, Kyaroikeidae). *Journal of Eukaryotic Microbiology* **53:** 407–419.

Ma R, **Ni B**, **Fan X**, **Warren A**, **Yin F**, **Gu F. 2016.** Ultrastructure observation on the cells at different life history stages of *Cryptocaryon irritans* (Ciliophora: Prostomatea), a parasitic ciliate of marine fishes. *Parasitology* **143:** 1479–1489.

Matthews BF, **Matthews RA**, **Burgess PJ. 1993.** *Cryptocaryon irritans* Brown, 1951 (Ichthyophthiriidae): the ultrastructure of the somatic cortex throughout the life cycle. *Journal of Fish Diseases* **16:** 339–349.

McFee WE, **Lipscomb TP. 2009.** Major pathologic findings and probable causes of mortality in bottlenose dolphins stranded in South Carolina from 1993 to 2006. *Journal of Wildlife Diseases* **45:** 575–593.

Medlin L, **Elwood HJ**, **Stickel S**, **Sogin ML. 1988.** The characterization of enzymatically amplified eukaryotic 16S-like rRNA-coding regions. *Gene* **71:** 491–499.

Meng Z, **Xu K**, **Dai R**, **Warren A. 2018.** Benthic ciliate diversity and community composition along water depth gradients: a comparison between the intertidal and offshore areas. *European Journal of Protistology* **65:** 31–41.

Moreira D, **Von der Heyden S**, **Bass D**, **López-García P**, **Chao E**, **Cavalier-Smith T. 2007.** Global eukaryote phylogeny: combined small- and large-subunit ribosomal DNA trees support monophyly of Rhizaria, Retaria and Excavata. *Molecular Phylogenetics and Evolution* **44:** 255–266.

Norman SA, **Goertz CE**, **Burek KA**, **Quakenbush LT**, **Cornick LA**, **Romano TA**, **Spoon T**, **Miller W**, **Beckett LA**, **Hobbs RC. 2012.** Seasonal hematology and serum chemistry of wild beluga whales (*Delphinapterus leucas*) in Bristol Bay, Alaska, USA. *Journal of Wildlife Diseases* **48:** 21–32.

Nylander JA. 2004. *MrModeltest v.2*. Uppsala: Evolutionary Biology Center, Uppsala University. Distributed by the author.

Page RDM. 1996. Treeview: an application to display phylogenetic trees on personal computers. *Computer Applications in the Biosciences* **12:** 357–358.

Pan X, **Bourland WA**, **Song WB. 2013.** Protargol synthesis an in-house protocol. *Journal of Eukaryotic Microbiology* **60:** 609–614.

Petz W, **Song W**, **Wilbert N. 1995.** Taxonomy and ecology of the ciliate fauna (Protozoa, Ciliophora) in the endopagial and pelagial of the Weddel Sea, Antarctica. *Stapfia* **40:** 1–223.

Posada D, **Crandall KA. 1998.** ModelTest: testing the model of DNA substitution. *Bioinformatics* **14:** 817–818.

Poynton SL, **Whitaker BR**, **Heinrich AB. 2001.** A novel trypanoplasm-like flagellate *Jarrellia atramenti* n. g., n. sp. (Kinetoplastida: Bodonidae) and ciliates from the blowhole of a stranded pygmy sperm whale *Kogia breviceps* (Physeteridae): morphology, life cycle and potential pathogenicity. *Diseases of Aquatic Organisms* **44:** 191–201.

Qu Z, **Wang C**, **Gao F**, **Li J**, **Al-Rasheid KAS**, **Hu X. 2015.** Taxonomic studies on seven species of *Dysteria* (Ciliophora, Cyrtophoria), including a description of *Dysteria paraprocera* sp. n. *European Journal of Protistology* **51:** 241–258.

Qu Z, **Ma H**, **Al-Farraj SA**, **Lin X**, **Hu X. 2017.** Morphology and molecular phylogeny of *Aegyria foissneri* sp. n. and *Lynchella minuta* sp. n. (Ciliophora, Cyrtophoria) from brackish waters of southern China. *European Journal of Protistology* **57:** 50–60.

Ronquist F, **Huelsenbeck JP. 2003.** MrBayes 3: Bayesian phylogenetic inference under mixed models. *Bioinformatics* **19:** 1572–1574.

Smith TG, **St. Aubin DJ**, **Hammill MO. 1992.** Rubbing behaviour of belugas, *Delphinapterus leucas*, in a high Arctic estuary. *Canadian Journal of Zoology* **70:** 2405–2409.

Sniezek JH, **Coats DW. 1996.** Stomatogenesis in *Kyaroikeus cetarius* (Dysteriina, Kyaroikeidae, n. fam.): clues to its systematic placement. *Journal of Eukaryotic Microbiology* **43:** 113–119.

Sniezek JH, **Coats DW**, **Small EB. 1995.** *Kyaroikeus cetarius* n. g., n. sp.: a parasitic ciliate from the respiratory tract of odonticete cetacea. *Journal of Eukaryotic Microbiology* **42:** 260–268.

Song W, **Wilbert N. 2000.** Ciliates from Antarctic sea ice. *Polar Biology* **23:** 212–222.

Song W, **Warren A**, **Hu X. 2009.** *Free-living ciliates in the Bohai and Yellow Seas, China*. Beijing: Science Press.

Stamatakis A, **Hoover P**, **Rougemont J. 2008.** A rapid bootstrap algorithm for the RAxML web servers. *Systematic Biology* **57:** 758–771.

Tamura K, **Peterson D**, **Peterson N**, **Stecher G**, **Nei M**, **Kumar S. 2011.** MEGA5: molecular evolutionary genetics analysis using maximum likelihood, evolutionary distance, and maximum parsimony methods. *Molecular Biology and Evolution* **28:** 2731–2739.

Wang P, **Wang Y**, **Wang C**, **Zhang T**, **Al-Farraj SA**, **Gao F. 2017.** Further consideration on the phylogeny of the Ciliophora: analyses using both mitochondrial and nuclear data with focus on the extremely confused class Phyllopharyngea. *Molecular Phylogenetics and Evolution* **112:** 96–106.

Warren A, **Patterson DJ**, **Dunthorn M**, **Clamp JC**, **Achilles-Day UEM**, **Aescht E**, **Al-Farraj SA**, **Al-Quraishy S**, **Al-Rasheid K**, **Carr M**, **Day JG**, **Dellinger M**, **El-Serehy HA**, **Fan Y**, **Gao F**, **Gao S**, **Gong J**, **Gupta R**, **Hu X**, **Kamra K**, **Langlois G**, **Lin X**, **Lipscomb D**, **Lobban CS**, **Luporini P**, **Lynn DH**, **Ma H**, **Macek M**, **Mackenzie-Dodds J**, **Makhija S**, **Mansergh RI**, **Martín-Cereceda M**, **McMiller N**, **Montagnes DJS**, **Nikolaeva S**, **Ong'ondo GO**, **Pérez-Uz B**, **Purushothaman J**, **Quintela-Alonso P**, **Rotterová J**, **Santoferrara L**, **Shao C**, **Shen Z**, **Shi X**, **Song W**, **Stoeck T**, **La Terza A**, **Vallesi A**, **Wang M**, **Weisse T**, **Wiackowski K**, **Wu L**, **Xu K**, **Yi Z**, **Zufall R**, **Agatha S. 2017.** Beyond the 'code': a guide to the description and documentation of biodiversity in ciliated protists (Alveolata, Ciliophora). *Journal of Eukaryotic Microbiology* **64:** 539–554.

Wilbert N. 1975. Eine verbesserte Technik der Protargolimprägnation für Ciliaten. *Mikrokosmos* **64:** 171–179.

Wirnsberger-Aescht E, **Foissner W**, **Foissner I. 1989.** Morphogenesis and ultrastructure of the soil ciliate *Engelmanniella mobilis* (Ciliophora, Hypotrichida). *European Journal of Protistology* **24:** 354–368.

Yi Z, **Song W**, **Clamp JC**, **Chen Z**, **Gao S**, **Zhang Q. 2009.** Reconsideration of systematic relationships within the order Euplotida (Protista, Ciliophora) using new sequences of the gene coding for small-subunit rRNA and testing the use of combined data sets to construct phylogenies of the *Diophrys*-complex. *Molecular Phylogenetics and Evolution* **50:** 599–607.

Zhao Y, **Yi Z**, **Warren A**, **Song W. 2018.** Species delimitation for the molecular taxonomy and ecology of the widely distributed microbial eukaryote genus *Euplotes* (Alveolata, Ciliophora). *Proceedings of the Royal Society B: Biological Sciences* **285:** 20172159.

SUPPORTING INFORMATION

Additional Supporting Information may be found in the online version of this article at the publisher's web-site.

Data S1. The data of blood routine examination in 2018.
Data S2. Cultivation data of *Kyaroikeus paracetarius* n. sp. *in vitro*.
Figure S1. Picture of the white beluga.
Figure S2. Pictures to show flocs of exfoliated epithelial tissue.
Figure S3. 3D scatter chart of morphometric data.
Video S1. Filming to show feeding, moving.